PAPER

Check for updates

Investigating charge-up and fragmentation dynamics of oxygen molecules after interaction with strong X-ray free-electron laser pulses†

G. Kastirke,[a] F. Ota,[b] D. V. Rezvan,[c] M. S. Schöffler, [iD][a] M. Weller,[a] J. Rist, [iD][a] R. Boll, [iD][d] N. Anders,[a] T. M. Baumann,[d] S. Eckart, [iD][a] B. Erk, [iD][e] A. De Fanis,[d] K. Fehre,[a] A. Gatton,[f] S. Grundmann, [iD][a] P. Grychtol, [iD][d] A. Hartung,[a] M. Hofmann,[a] M. Ilchen,[cd] C. Janke,[a] M. Kircher,[a] M. Kunitski,[a] X. Li,[g] T. Mazza,[d] N. Melzer, [iD][a] J. Montano,[d] V. Music,[cd] G. Nalin, [iD][a] Y. Ovcharenko,[d] A. Pier,[a] N. Rennhack,[d] D. E. Rivas,[d] R. Dörner,[a] D. Rolles, [iD][g] A. Rudenko,[g] Ph. Schmidt, [iD][cd] J. Siebert,[a] N. Strenger,[a] D. Trabert,[a] I. Vela-Perez,[a] R. Wagner,[d] Th. Weber, [iD][h] J. B. Williams,[i] P. Ziolkowski,[d] L. Ph. H. Schmidt,[a] A. Czasch,[a] Y. Tamura,[b] N. Hara,[b] K. Yamazaki, [iD][j] K. Hatada,[b] F. Trinter, [iD][ek] M. Meyer,[d] K. Ueda,[lm] Ph. V. Demekhin [iD][c] and T. Jahnke ★[d]

During the last decade, X-ray free-electron lasers (XFELs) have enabled the study of light–matter interaction under extreme conditions. Atoms which are subject to XFEL radiation are charged by a complex interplay of (several subsequent) photoionization events and electronic decay processes within a few femtoseconds. The interaction with molecules is even more intriguing, since intricate nuclear dynamics occur as the molecules start to dissociate during the charge-up process. Here, we demonstrate that by analyzing photoelectron angular emission distributions and kinetic energy release of charge states of ionic molecular fragments, we can obtain a detailed understanding of the charge-up and fragmentation dynamics. Our novel approach allows for gathering such information without the need of complex *ab initio* modeling. As an example, we provide a detailed view on the processes happening on a femtosecond time scale in oxygen molecules exposed to intense XFEL pulses.

1 Introduction

Accessing atomic and molecular length and time scales is a key necessity of many disciplines in physics, chemistry, and biology. Accordingly, several experimental approaches have been developed during the last decades, targeting different aspects of this challenge. For example, the geometrical structure even of very large molecules nowadays can be retrieved routinely by means of X-ray diffraction in cases, where nano-crystals of the examined molecules can be created.[1] Studying single molecules in the gas phase[2,3] poses even more challenges than X-ray diffraction methods, because they suffer from the weak scattering properties of light elements as, *e.g.*, hydrogen atoms. Accordingly, several alternative approaches employing electron waves as

[a] *Institut für Kernphysik, Goethe-Universität, Max-von-Laue-Straße 1, 60438 Frankfurt am Main, Germany*

[b] *Department of Physics, University of Toyama, Gofuku 3190, Toyama 930-8555, Japan*

[c] *Institut für Physik und CINSaT, Universität Kassel, Heinrich-Plett-Straße 40, 34132 Kassel, Germany. E-mail: demekhin@physik.uni-kassel.de*

[d] *European XFEL, Holzkoppel 4, 22869 Schenefeld, Germany. E-mail: till.jahnke@xfel.eu*

[e] *Deutsches Elektronen-Synchrotron DESY, Notkestraße 85, 22607 Hamburg, Germany*

[f] *SLAC National Accelerator Laboratory, Menlo Park, California 94025, USA*

[g] *J.R. Macdonald Laboratory, Department of Physics, Kansas State University, Manhattan, Kansas 66506, USA*

[h] *Lawrence Berkeley National Laboratory, Chemical Sciences Division, Berkeley, California 94720, USA*

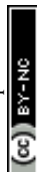[i] *Department of Physics, University of Nevada, Reno, Nevada 89557, USA*

[j] *RIKEN Center for Advanced Photonics, RIKEN, 2-1 Hirosawa, Wako, Saitama, 351-0198, Japan*

[k] *Molecular Physics, Fritz-Haber-Institut der Max-Planck-Gesellschaft, Faradayweg 4-6, 14195 Berlin, Germany*

[l] *Institute of Multidisciplinary Research for Advanced Materials, Tohoku University, Katahira 2-1-1, Aoba-ku, Sendai 980-8577, Japan*

[m] *Department of Chemistry, Tohoku University, 6-3 Aramaki Aza-Aoba, Aoba-ku, Sendai, 980-8578, Japan. E-mail: kiyoshi.ueda@tohoku.ac.jp*

† Electronic supplementary information (ESI) available. See DOI: **https://doi.org/10.1039/d2cp02408j**

This journal is © the Owner Societies 2022

Phys. Chem. Chem. Phys., 2022, **24**, 27121–27127 | **27121**

molecular structure probes (thus, compensating this deficiency) have emerged.[4–9]

A particular variant of electron diffraction imaging uses molecular photoelectrons to sample the structure of molecules. Studies of so-called molecular-frame photoelectron angular distributions (MFPADs) record the emission pattern of photoelectrons in a molecular frame of reference.[10] This angular distribution is a result of the photoelectron wave being scattered by the molecular potential as it propagates through the molecule. It is therefore not only sensitive to the molecular geometry but also for instance to the electron's wavelength, the initial state of the electron, the emission site inside the molecule (in case of core-electron emission), and the polarization properties of the ionizing light. Since the 90s of the last century, many experiments using synchrotron radiation investigated different aspects of such MFPADs,[11] as their sensitivity to molecular vibrations[12] and molecular shape resonances,[13] to the bound-state momentum-space wave function of the emitted electron,[14] and even the temporal response of an electronic orbital to ionizing radiation.[15] With respect to extracting geometrical structure information, so-called polarization-averaged MFPADs (PA-MFPADs) are favorable: Williams et al. demonstrated that in special cases the MFPAD of carbon K-shell electrons emitted from methane molecules directly resembles the three-dimensional molecular geometry,[16] and Fukuzawa et al. showed in general that the full information on molecular bond lengths is encoded in such PA-MFPADs.[17]

With the advent of X-ray free-electron lasers (XFELs), a further intriguing aspect emerged. XFELs are capable of producing ultra-bright pulses of X-rays with shortest duration in the regime of a few tens of femtoseconds. This opened the route to time-resolved studies, where MFPADs record snapshots of nuclear motion occurring inside a molecule.[18]

Recently, Kastirke et al. demonstrated a first step towards obtaining such molecular movies using an XFEL.[19] They triggered the dissociation of an oxygen molecule by absorption of an X-ray photon. The PA-MFPAD of a secondary photoelectron (which was emitted during the fragmentation process) depicted a fingerprint of the increasing internuclear distance during the fragmentation. In the present paper, we depict results that go one step further. By applying a novel analysis approach of extracting information from the PA-MFPADs, we were able to trace the femtosecond charge-up and fragmentation dynamics of the oxygen molecule occurring during the illumination with an ultra-short free-electron X-ray pulse.

In pioneering work, Young et al. demonstrated that the interaction of X-ray free-electron laser light with atoms gives rise to a complex interplay of multiple photoionization and Auger decay events[20] which was then further studied, revealing the role of resonances in such charge-up processes in atoms[21] and recently also in molecules.[22,23] In case of molecules, a further dimension of complexity is added to this charge-up process, as typically additional nuclear dynamics are triggered as soon as the first charges are generated and the molecules start to dissociate.[24] If, for instance, during a XFEL pulse an oxygen molecule absorbs two X-ray photons of a sufficient

energy, it ends up typically in a total charge state of four, as both inner-shell photoionization events (P) trigger a subsequent Auger decay (A). However, the exact sequence may differ from case to case: If the two ionization events occur prior to Auger decay, the photo-process is termed double core-hole creation and labelled as a 'PPAA' sequence. This can also be triggered by single-photon absorption at sufficiently high photon energies (see, e.g., ref. 25) which however precludes access to the evolving system. The double core-hole can be either located at a single atom of the molecule (single-site double core-hole), or the two electrons may emerge from different atoms (two-site double core-hole).[26] If the second ionization happens after a first Auger decay, this process is labelled as a 'PAPA' sequence of consecutive photoionization and Auger decay events. In addition, the absorption of two photons may even yield a total molecular charge of five, if an additional electron is shaken off during one of the photoionization or Auger decay events. In all above-mentioned cases, the molecule starts to fragment as soon as two vacancies have been created. Adding further complexity, charge-transfer processes may occur during the fragmentation as long as the internuclear distances are not yet too large.[22] Such charge transfer is an important aspect of chemical reactions as it changes their path and outcome. It occurs on ultrafast time scales and is at the heart of investigations of fundamental processes of modern ultrafast science. The aim of this paper is to demonstrate how these processes can be examined in an experiment in large detail by employing coincident imaging of emitted electrons and molecular ionic fragments.

For our study, we employed the SQS-REMI end-station located at the European X-ray free-electron laser facility.[27] The COLTRIMS reaction microscope[28,29] was used to measure in coincidence the ionic fragments and at least one of the emitted photoelectrons occurring during the interaction of the XFEL light with single oxygen molecules in the gas phase. The X-ray pulses had an initial pulse energy of 2.4 mJ and were attenuated to (30 ± 5) µJ using a nitrogen-containing gas absorber. Taking into account the beamline transmission,[30] this resulted in pulse energies of (14 ± 2) µJ on target in a focus of a size of approximately 1×2 µm^2. The pulse duration is estimated to be approximately 25 fs, based on the electron-bunch charge of 250 pC. More details on the experimental setup are provided in ref. 19 and 31. Accordingly, from our experiment we obtain the following information for each photoreaction event: The kinetic energy of the photoelectron, its emission direction with respect to the molecular axis, the kinetic energy of the fragment ions, their charge state, and their emission directions. As will be demonstrated below, this information can be employed to follow the route of the charge-up and fragmentation dynamics of O_2.

2 Results and discussion

As a starting point, we analyze the electron energy spectra (obtained after irradiating the molecules with XFEL pulses of
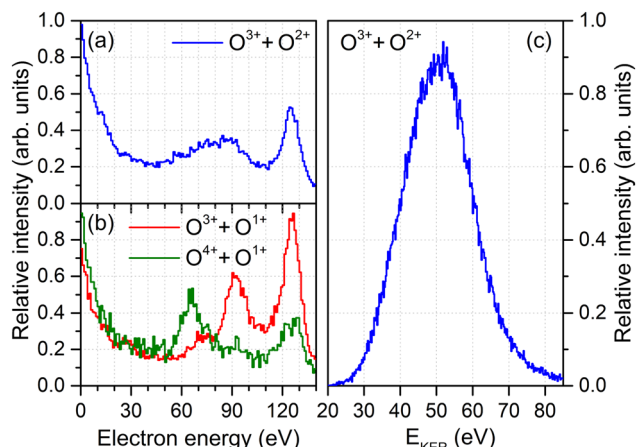
27122 | *Phys. Chem. Chem. Phys.*, 2022, **24**, 27121–27127

This journal is © the Owner Societies 2022

Fig. 1 Electron energy spectra of O_2 irradiated with intense XFEL pulses ($h\nu$ = 665 eV) recorded in coincidence with the O^{3+} + O^{2+} final state (panel a), the O^{3+} + O^{1+} and the O^{4+} + O^{1+} final states (panel b), together with the ion kinetic energy release spectrum for the O^{3+} + O^{2+} case (panel c). The relative strength of the three breakup channels is O^{3+} + O^{2+}: 1, O^{3+} + O^{1+}:0.66, and O^{4+} + O^{1+}:0.14.

an energy of $h\nu$ = 665 eV) for different fragmentation channels shown in Fig. 1(a) and (b). The spectrum for the O^{3+} + O^{2+} channel, which is of primary interest of this work, is shown in Fig. 1(a). It gives us the ability to distinguish between the first and second emitted photoelectron: The main line of the first photoelectron occurs at a kinetic energy of approximately 130 eV and a feature of multiple photoionization, which can be attributed to the second photoelectron in the PAPA sequence, is seen in a range of 55 eV to 110 eV.[19] This feature is, however, much broader than expected for the PAPA process.

In order to understand its origin, we examine other fragmentation channels in Fig. 1(b). There, the red curve depicts the energy spectrum of the O^{3+} + O^{1+} final state. A clear peak belonging to the PAPA process is visible at an energy of about 90 eV. The most probable pathway to generate these electrons (and this molecular charge state) is a photoionization with subsequent Auger decay (generating the O^{1+} + O^{1+} intermediate state) followed by a second photoionization and Auger decay during the fragmentation of the molecule (resulting in the final O^{3+} + O^{1+} state). The green curve in Fig. 1(b) shows the corresponding electron energy spectrum if the O^{4+} + O^{1+} final state is created. In this case, the PAPA peak moves to lower energies of about 65 eV. This suggests that the O^{4+} + O^{1+} state is created, to large extent, by an additional shake-off event in the second photoionization step. This diminishes the energy of that second photoelectron by the energy needed to release an additional electron. Thus, after the first photoionization and Auger decay event, the molecule is further photoionized, emits a shake-off electron and an Auger electron, adding in total three more charges: O^{1+} + O^{1+} → O^{4+} + O^{1+}. These shake-off electrons are visible in the increase of the respective contribution below 20 eV, as compared to the other channel [*cf.*, green and red curves in Fig. 1(b)].

These observations imply that the broad feature observable in the electron energy spectrum obtained for the O^{3+} + O^{2+} channel in Fig. 1(a) may consist of a mixture of both charge-up schemes.

Electrons generated by a regular second photoionization event are responsible for the high-energy part of that feature, whereas the other ionization pathway, in which the second photoionization was accompanied by shake-off, contributes to the low-energy part. However, since the molecule is five-fold charged in the final state, in the former case an additional shake-off event occurred during the first photoionization step, and the second ionization step of this route reads: O^{1+} + O^{2+} → O^{3+} + O^{2+}. This line of arguments would suggest that if the shake-off took place during the second photoionization event, the final charge state of the molecule should be O^{4+} + O^{1+}. However, we barely observe the O^{4+} + O^{1+} charge state in our experiment, which indicates that this channel is either not as probable as the O^{3+} + O^{2+} channel, or that this transient charge state relaxes further into O^{3+} + O^{2+} *via* charge transfer as long as the internuclear separation is not too large. Under the given experimental conditions, such short internuclear distances are present for a large part of the pulse duration. The classical 'over-the-barrier' charge-transfer model of ref. 32 suggests that this happens efficiently at internuclear distances of up to $R \leq 3R_{eq} \approx 6.85$ a.u., where R_{eq} is the equilibrium internuclear distance. Here, the total energy of O^{4+} + O^{1+} is still larger than the potential energy of O^{3+} + O^{2+}. In what follows, we refer to the different routes yielding O^{3+} + O^{2+} by indicating whether in the second photoionization step only the photoelectron was emitted or two electrons were emitted by shake-off photoionization. Accordingly, we label the photoionization route O^{1+} + O^{2+} → O^{3+} + O^{2+} as the main pathway and the O^{1+} + O^{1+} → O^{3+} + O^{2+} case as the satellite channel.

The nuclear dynamics during the charge-up are dominated by the fragmentation of the molecule. Information on the internuclear separation R of the two ionic fragments at the instant of the secondary O 1s photoionization is imprinted on the ions' kinetic energy release E_{KER}. In order to interconnect R and E_{KER}, a very simple classical Coulomb-explosion model[19] can be applied. It assumes a sequence of the following steps: At first, the primary O 1s photoionization and subsequent Auger decay take place at the equilibrium separation R_{eq} which form the O^{z_l+} + O^{z_r+} charge state (with z_l and z_r denoting the possible charge states at the left and right side of the molecule). Thereafter, the O–O bond elongates on the repulsive potential $z_l z_r/r$ (with r being the distance between the two charges) until the internuclear separation R is reached, where the secondary O 1s photoionization and an immediate Auger decay take place forming the final $O^{z_l'+}$ + $O^{z_r'+}$ charge state. Finally, the resulting-state fragments on the repulsive potential $z_l' z_r'/r$ of the two ions are detected. The resulting kinetic energy release E_{KER} and internuclear distance R are, thus, related as:

$$E_{KER} = \frac{z_l z_r}{R_{eq}} + \frac{z_l' z_r' - z_l z_r}{R} \quad \text{or} \quad R = \frac{z_l' z_r' - z_l z_r}{E_{KER} - z_l z_r/R_{eq}}. \quad (1)$$

To this end, however, it is not clear to what extent this simplistic model is capable of capturing the complex charge-up dynamics. For example, synchrotron work on O_2 molecules on low-final-charge states depicts very complex (*i.e.*, feature-rich)

kinetic energy release distributions which can be attributed to a multitude of accessible intermediate states.[33] As depicted in Fig. 1(c), we observe a kinetic energy release of the $O^{3+} + O^{2+}$ fragments in a range of about 30 eV $< E_{KER} < $ 75 eV in the experiment, which exhibits mainly a single peak. From the solitary KER distribution the ionization pathways and different intermediate states, thus, cannot be disentangled.

PA-MFPADS do allow to unravel the full charge-up and bond-breaking dynamics as we will show in the following. Fig. 2 depicts examples of such distributions for different distances between the oxygen atoms as obtained from a full theoretical modeling employing the single-center method.[34,35] The calculations were performed as described in detail in our previous works on this molecule.[19,31] The modeled angular distributions have been normalized to the forward peak pointing towards the doubly charged oxygen ion. While the details of the PA-MFPAD depend strongly on the internuclear distance R, a closer inspection of the photoelectron flux towards the singly charged oxygen ion, which after the photoionization and Auger decay becomes triply charged, shows an oscillatory trend with respect to R. In particular, starting from a minimum at the largest distance of 6 a.u., several minima and maxima in the emission pattern emerge in the direction labeled as 'Backward' in Fig. 2 for smaller internuclear separations (*i.e.*, from yellow- to blue-colored MFPADs).

This behavior of the backward peak of the PA-MFPAD can be explained already within a simplified theoretical model.[36,37] It employs the single-channel, single-scattering, plane-wave, and muffin-tin approximations. It also includes a superposition of a direct electron wave with momentum k emitted from the left
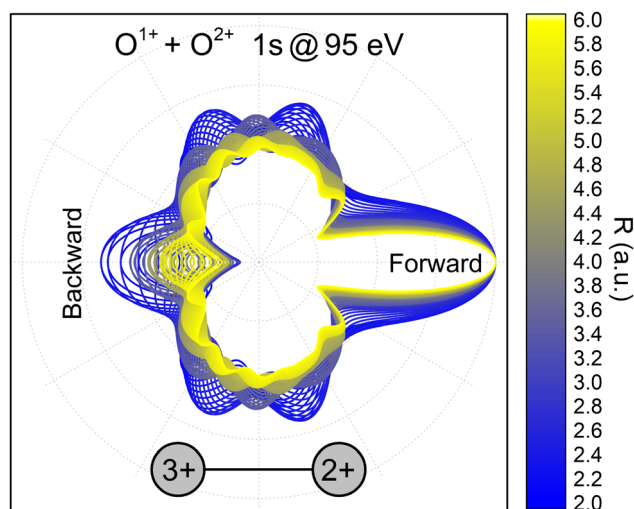

Fig. 2 Polarization-averaged MFPADs of the second 1s photoelectron, computed in the relaxed-core Hartree–Fock approximation at different internuclear separations for the $O^{1+} + O^{2+} \rightarrow O^{3+} + O^{2+}$ channel. After the second photoionization and Auger decay, the left singly charged oxygen ion becomes triply charged. An electron energy of 95 eV was used in the calculations, as these electrons represent the high-energy part of the broad feature in Fig. 1(a). The PA-MFPADs are normalized to the forward peak. The color encodes the internuclear separation between the two oxygen ions at the instant of the photoionization.
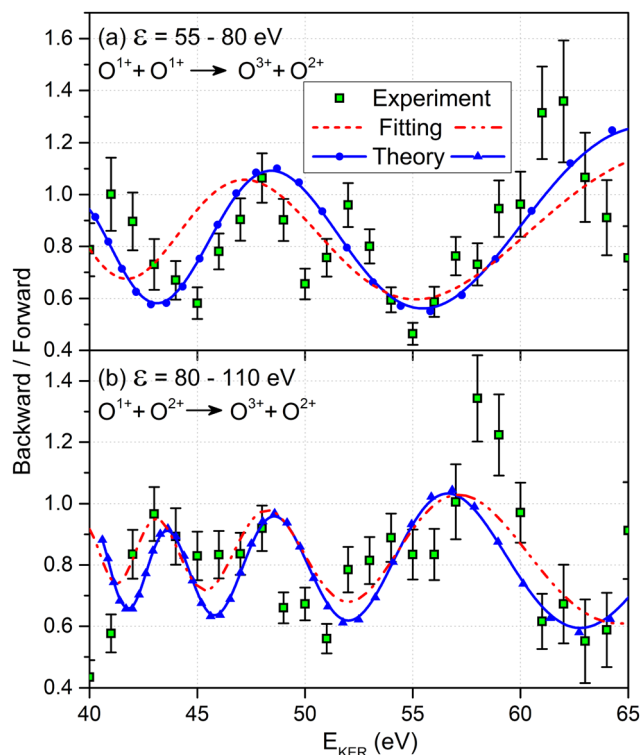
oxygen ion in Fig. 2 with an electron wave which occurs due to scattering at the second oxygen ion at the right. Using the site T-matrix expansion,[38,39] we obtain the following analytic expression for the polarization-averaged differential probability of the 1s photoionization of the left oxygen atom O_l of a fixed-in-space oxygen molecule (see ref. 36 and 37 on details of the derivation):

$$\left\langle I_k^{O_l}(\theta) \right\rangle_\varepsilon \propto 1 + \frac{2\Re\left[e^{ikR(1-\cos\theta)} f^{O_r}(k,\theta)\right]}{R}\cos\theta + \frac{\left|f^{O_r}(k,\theta)\right|^2}{R^2}. \quad (2)$$

Here, R is the internuclear distance and θ is the electron emission angle with respect to the molecular axis. The first term in eqn (2) represents the direct photoemission from the O_l atom and its spherical symmetry owing to the polarization average. The third term describes the single scattering by the O_r atom with the amplitude $f^{O_r}(k, \theta)$. The second term corresponds to the interference between the direct and scattered waves, and it creates the flower-shape petals in the PA-MFPADs, *i.e.*, it creates maxima and minima at the emission angles in between the forward and backward directions in the computed distributions.

Substituting $\theta = 0$ in eqn (2) removes the phase factor exp[ikR $(1 - \cos\theta)$] from the forward intensity, while for $\theta = \pi$, the backward intensity oscillates as a function of $2kR$.[40]

It is straightforward to obtain the following parametrization of the ratio of the backward to forward intensities:

$$\eta_k(R) = \frac{\left\langle I_k^{O_l}(\pi) \right\rangle_\varepsilon}{\left\langle I_k^{O_l}(0) \right\rangle_\varepsilon} = \frac{a_k(R)}{R}\cos\left[2kR + \phi_k^{O_r}(\pi)\right] + b_k(R), \quad (3)$$

with known coefficients $a_k(R)$, $b_k(R)$, and the back-scattering phase $\phi_k^{O_r}(\pi)$. One can see that this ratio oscillates with $\cos(2kR)$, *i.e.*, with the phase accumulated by the scattered wave on its way $2R$ from the O_l to O_r atoms and back.

We now analyze the backward–forward ratio of the PA-MFPADs given by eqn (3) of the secondary photoelectron as a function of E_{KER} for two regions with low $\varepsilon = $ 55–80 eV and high $\varepsilon = $ 80–110 eV electron energies, which we attributed previously to the satellite and main pathways. The corresponding results are shown in Fig. 3(a) and (b), respectively, as symbols with error bars for the experiment. The measured ratios possess clear oscillations in a wide range of the measured kinetic energy release E_{KER}. The internuclear separation R at the instant of the second photoionization event is linked with E_{KER} *via* eqn (1). In order to support our assumption that photoelectrons with higher kinetic energies are mainly produced by the main pathway ($O^{1+} + O^{2+} \rightarrow O^{3+} + O^{2+}$) and those with lower energy by the satellite channel ($O^{1+} + O^{1+} \rightarrow O^{3+} + O^{2+}$), we apply our simplified analytical model and perform a fitting of the ratios determined by the experiment using eqn (3). We assume the coefficients $a_k(R)$, $b_k(R)$, and the back-scattering phase $\phi_k^{O_r}(\pi)$ to be constant parameters for each photoionization channel. Furthermore, we use average photoelectron kinetic energies of $\varepsilon = $ 95 eV and $\varepsilon = $ 67.5 eV for the main and satellite

27124 | *Phys. Chem. Chem. Phys.*, 2022, **24**, 27121–27127

This journal is © the Owner Societies 2022

Fig. 3 Comparison between the experimental backward-to-forward ratios (symbols with error bars), measured for the $O^{3+} + O^{2+}$ final charge state and the photoelectron kinetic energy ranges of: (a) $\varepsilon = 55-80$ eV and (b) $\varepsilon = 80-110$ eV. The fitted ratios (broken curves) and the *ab initio* theoretical results (solid curves with symbols) represent individual contributions from the main channel $O^{1+} + O^{2+} \rightarrow O^{3+} + O^{2+}$ in panel (b) and from the satellite channel $O^{1+} + O^{1+} \rightarrow O^{3+} + O^{2+}$ in panel (a). To facilitate comparison with the experiment, the *ab initio* ratios include a constant background of +0.5.

channels. In order to interrelate the internuclear distance R with E_{KER} *via* eqn (1), we used $(z_l, z_r; z'_l, z'_r) = (1, 1; 3, 2)$ for the satellite channel $O^{1+} + O^{1+} \rightarrow O^{3+} + O^{2+}$ in Fig. 3(a) and $(z_l, z_r; z'_l, z'_r) = (1, 2; 3, 2)$ for the main channel $O^{1+} + O^{2+} \rightarrow O^{3+} + O^{2+}$ in Fig. 3(b). The results are depicted in Fig. 3 by the dashed (red) curves (see legend). Details on the fitting procedure are summarized in the ESI.†

Our findings are furthermore confirmed as we extract the corresponding ratios from our full *ab initio* calculations (solid blue curves with symbols in Fig. 3). The same assumption for the transformation of R to E_{KER} *via* eqn (1) and the same mean photoelectron kinetic energies were used in our calculations. Both the *ab initio* theoretical results and the results employing our analytical model reproduce the experimentally observed backward–forward emission ratios. This supports that our assumption on the decay path generating low- and high-energy photoelectrons in producing the $O^{3+} + O^{2+}$ charge state as being correct. We attribute the deviation of our simple scattering model and the *ab initio* calculations to remaining contributions from a multiple scattering of the outgoing photoelectron wave.

After having substantiated our interpretation of the two charge-up routes leading to $O^{3+} + O^{2+}$ and determined the

connection between E_{KER} and internuclear distance R, we will now provide information on the time-domain properties of the charge-up process as a final step of our analysis. We use the same simple Coulomb-explosion model to examine the temporal evolution of the internuclear distances in the intermediate states $O^{1+} + O^{1+}$ and $O^{1+} + O^{2+}$ during the XFEL pulse. The Newtonian equation of motion for the O–O separation along the bond in the $O^{z_l+} + O^{z_r+}$ intermediate state reads

$$\mu \frac{d^2 R}{dT^2} = \frac{z_l z_r}{R^2}, \quad (4)$$

where μ is the reduced mass of the molecule and T is the time delay between the first and second photoionization event. The solution of eqn (4) with the boundary conditions $R|_{T=0} = R_{eq}$ and $dR/dT|_{T=0} = 0$ reads:

$$T(R) = \sqrt{\frac{\mu}{2 z_l z_r}} \left[\sqrt{R R_{eq}(R - R_{eq})} - \frac{R_{eq}^{3/2}}{2} \ln \left(\frac{\sqrt{R} - \sqrt{R - R_{eq}}}{\sqrt{R} + \sqrt{R - R_{eq}}} \right) \right] \quad (5)$$

The results of $T(R)$ simulated by eqn (5) and those of $T(E_{KER})$ by eqn (1) and (5) are depicted in Fig. 4. As one can see, it takes about 18 fs to yield a kinetic energy release as low as 40 eV (broken curves in Fig. 4). During that time, the O–O bond length increases to about 7 a.u. for the $O^{1+} + O^{2+}$ and 5 a.u. for the $O^{1+} + O^{1+}$ channels, respectively. These results suggest that the XFEL pulse with a duration of 20–30 fs (FWHM) indeed creates O_2^{5+} ions and our kinetic energy release range of 40 eV $\leq E_{KER} \leq$ 65 eV used in Fig. 3 for the $O^{2+} + O^{3+}$ charge state was reasonable.
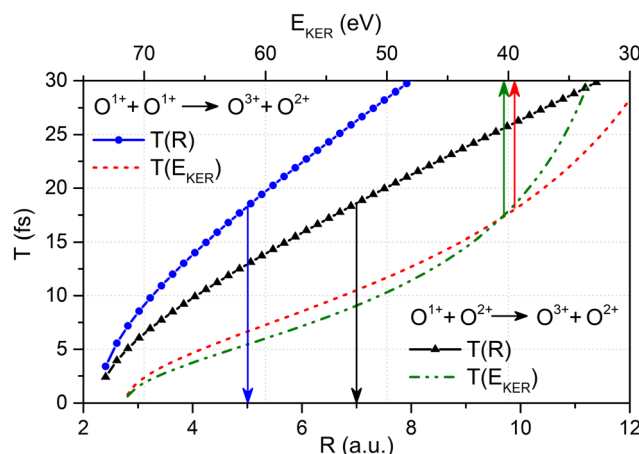

Fig. 4 The relation between the O–O bond length R and the time delay T between first and second ionization event given by eqn (5) (solid curves with symbols, refer to the lower horizontal scale) together with the relation between E_{KER} and the time delay T between first and second ionization event obtained *via* eqn (5) with the O–O bond length R given as a function of E_{KER} *via* eqn (1) (broken curves, refer to the upper horizontal scale) for the $O^{1+} + O^{2+} \rightarrow O^{3+} + O^{2+}$ main and the $O^{1+} + O^{1+} \rightarrow O^{3+} + O^{2+}$ satellite channel, respectively (see legends).

This journal is © the Owner Societies 2022

Phys. Chem. Chem. Phys., 2022, **24**, 27121–27127 | **27125**

3 Conclusions

In conclusion, we have demonstrated that the charge-up and fragmentation dynamics of a small molecule interacting with intense ultra-short X-ray pulses can be examined in intriguing detail by employing COLTRIMS reaction microscopy. The information content of our electron-ion coincidence measurement reveals the charge-up during the photo-dissociation process and its time evolution, while applying very modest assumptions and simplified scattering models. Our *ab initio* treatment of the emitted photoelectrons confirms this assessment. Our work suggests that charge-up and fragmentation dynamics of even larger molecules should be addressable with similar analysis concepts. In addition, future time-resolved studies using X-ray pump/X-ray probe schemes for the two photoionization events could directly investigate the process described in this article and confirm that PA-MFPADs in connection with additional observables measured in coincidence are a suitable tool for obtaining a detailed understanding of molecular charge-up processes.

Author contributions

All authors except for P. V. D., D. V. R., F. O., Y. T., N. H., K. Y., and K. H. have participated in the experiment. D. V. R. and P. V. D. performed the theoretical calculations. T. J., A. C., and G. K.: Data analysis. F. O., K. Y., K. H., K. U., T. J., and P. V. D.: Interpretation of the data. F. O., Y. T., N. H., K. Y., K. H., and K. U. conceived the simplified model. F. O., Y. T., N. H., K. Y., and K. H. performed the simulations based on the simplified model. P. V. D., T. J., F. O., K. Y., K. H., and K. U. drafted the manuscript. All authors discussed the results and revised/contributed to the manuscript.

Conflicts of interest

There are no conflicts to declare.

Acknowledgements

Notes and references

1 H. N. Chapman, *et al.*, *Nature*, 2011, **470**, 73–77.
2 J. Küpper, *et al.*, *Phys. Rev. Lett.*, 2014, **112**, 083002.
3 M. P. Minitti, *et al.*, *Phys. Rev. Lett.*, 2015, **114**, 255501.
4 T. Gruene, *et al.*, *Angew. Chem., Int. Ed.*, 2018, **57**, 16313–16317.
5 C. J. Hensley, J. Yang and M. Centurion, *Phys. Rev. Lett.*, 2012, **109**, 133202.
6 B. Wolter, *et al.*, *Science*, 2016, **354**, 308–312.
7 J. Yang, *et al.*, *Science*, 2018, **361**, 64–67.
8 T. J. A. Wolf, *et al.*, *Nat. Chem.*, 2019, **11**, 504–509.
9 E. G. Champenois, *et al.*, *Science*, 2021, **374**, 178–182.
10 A. Landers, *et al.*, *Phys. Rev. Lett.*, 2001, **87**, 013002.
11 A. V. Golovin, N. A. Cherepkov and V. V. Kuznetsov, *Z. Phys. D: At., Mol. Clusters*, 1992, **24**, 371–375.
12 J. Adachi, K. Hosaka, S. Furuya, K. Soejima, M. Takahashi, A. Yagishita, S. K. Semenov and N. A. Cherepkov, *Phys. Rev. Lett.*, 2003, **91**, 163001.
13 E. Shigemasa, J. Adachi, K. Soejima, N. Watanabe, A. Yagishita and N. A. Cherepkov, *Phys. Rev. Lett.*, 1998, **80**, 1622.
14 M. Waitz, *et al.*, *Nat. Commun.*, 2017, **8**, 2266.
15 S. Grundmann, *et al.*, *Science*, 2020, **370**, 339–341.
16 J. B. Williams, *et al.*, *Phys. Rev. Lett.*, 2012, **108**, 233002.
17 H. Fukuzawa, *et al.*, *J. Chem. Phys.*, 2019, **150**, 174306.
18 R. Boll, *et al.*, *Phys. Rev. A*, 2013, **88**, 061402(R).
19 G. Kastirke, *et al.*, *Phys. Rev. X*, 2020, **10**, 021052.
20 L. Young, *et al.*, *Nature*, 2010, **466**, 56–61.
21 B. Rudek, *et al.*, *Nat. Photonics*, 2012, **6**, 858–865.
22 A. Rudenko, *et al.*, *Nature*, 2017, **546**, 129–132.

27126 | *Phys. Chem. Chem. Phys.*, 2022, **24**, 27121–27127

This journal is © the Owner Societies 2022

23 X. Li, *et al.*, *Phys. Rev. A*, 2022, **105**, 053102.

24 X. Li, *et al.*, *Sci. Rep.*, 2021, **11**, 505.

25 G. Goldsztejn, *et al.*, *Phys. Rev. A*, 2017, **96**, 012513.

26 N. Berrah, *et al.*, *Proc. Natl. Acad. Sci. U. S. A.*, 2011, **108**, 16912–16915.

27 T. Tschentscher, C. Bressler, J. Grünert, A. Madsen, A. P. Mancuso, M. Meyer, A. Scherz, H. Sinn and U. Zastrau, *Appl. Sci.*, 2017, **7**, 592.

28 J. Ullrich, R. Moshammer, A. Dorn, R. Dörner, L. Ph. H. Schmidt and H. Schmidt-Böcking, *Rep. Prog. Phys.*, 2003, **66**, 1463.

29 T. Jahnke, Th. Weber, T. Osipov, A. L. Landers, O. Jagutzki, L. Ph. H. Schmidt, C. L. Cocke, M. H. Prior, H. Schmidt-Böcking and R. Dörner, *J. Electron Spectrosc. Relat. Phenom.*, 2004, **141**, 229–238.

30 T. Mazza, T. M. Baumann, R. Boll, A. De Fanis, P. Grychtol, M. Ilchen, J. Montano, V. Music, Y. Ovcharenko, N. Rennhack, D. E. Rivas, P. Rörig, P. Schmidt, S. Usenko, P. Ziolkowski, D. La Civita, M. Vannoni, H. Sinn, B. Keitel,

E. Plönjes, K. Mann, B. Schäfer, S.-K. Son and M. Meyer, *J. Synchrotron Radiat.*, 2022, to be submitted.

31 G. Kastirke, *et al.*, *Phys. Rev. Lett.*, 2020, **125**, 163201.

32 H. Ryufuku, K. Sasaki and T. Watanabe, *Phys. Rev. A*, 1980, **21**, 745.

33 Z. Bao, R. F. Fink, O. Travnikova, D. Céolin, S. Svensson and M. N. Piancastelli, *J. Phys. B: At., Mol. Opt. Phys.*, 2008, **41**, 125101.

34 Ph. V. Demekhin, A. Ehresmann and V. L. Sukhorukov, *J. Chem. Phys.*, 2011, **134**, 024113.

35 S. A. Galitskiy, A. N. Artemyev, K. Jänkälä, B. M. Lagutin and Ph. V. Demekhin, *J. Chem. Phys.*, 2015, **142**, 034306.

36 F. Ota, K. Yamazaki, D. Sébilleau, K. Ueda and K. Hatada, *J. Phys. B: At., Mol. Opt. Phys.*, 2021, **54**, 024003.

37 F. Ota, K. Hatada, D. Sébilleau, K. Ueda and K. Yamazaki, *J. Phys. B: At., Mol. Opt. Phys.*, 2021, **54**, 084001.

38 J. S. Faulkner and G. M. Stocks, *Phys. Rev. B*, 1980, **21**, 3222.

39 K. Hatada, K. Hayakawa, M. Benfatto and C. R. Natoli, *J. Phys.: Condens. Matter*, 2010, **22**, 185501.

40 B. Zimmermann, *et al.*, *Nat. Phys.*, 2008, **4**, 649–655.

This journal is © the Owner Societies 2022

Phys. Chem. Chem. Phys., 2022, **24**, 27121–27127 | **27127**